Journal of Superconductivity and Novel Magnetism (2024) 37:565–571
https://doi.org/10.1007/s10948-023-06686-2

Current-Induced Domain Wall NOT Gate Logic Operation via Chirality Flipping by Exploiting Walker Breakdown

Vemuru Haragopal[1] · Rohan Jaiswal[1] · Vijayanandhini Kannan[1] · Chandrasekhar Murapaka[2] · Wen Siang Lew[3]

Received: 27 July 2023 / Accepted: 26 December 2023 / Published online: 27 January 2024

Abstract
Current-induced domain wall (DW) motion in ferromagnetic nanostructures is an important research area to realize spin-based logic devices. Using micromagnetic simulations, we have designed and demonstrated a NOT gate logic operation via DW chirality flipping in a ferromagnetic nanostructure with an anti-dot. The DW chirality flipping is due to the Walker breakdown occurring at the anti-dot structure. The DW configuration transforms from a transverse DW (TDW) to an anti-vortex DW and back to TDW, however, with opposite chirality when driven by a particular current density. The device is capable of bidirectional operation, wherein the DW driven in both directions undergoes chirality flipping. The DW speed is a critical parameter for the logic operation. The dimensions of the anti-dot govern the DW speed; thus, the successful operation is seen only below the critical anti-dot width. Moreover, the DW needs to travel a certain distance before it can undergo Walker breakdown, making the anti-dot length also a key parameter. Finally, the current density is a pivotal factor in the logic-gate operation. At relatively lower current densities, the DW does not undergo Walker breakdown, whereas it may undergo Walker breakdown with several transformations before it reaches the output at higher current densities. We have shown the window of successful NOT gate logic operation, as a function of anti-dot width, length, and current density.

Keywords Domain wall · Spin-transfer torque · Domain wall chirality · NOT gate logic · Walker breakdown

1 Introduction

Domain walls (DWs) in ferromagnetic nanostructures have shown great promise for the realization of novel spintronic-based memory and logic devices [1–4]. The DW that separate two domains in ferromagnets are also interesting for fundamental understanding of magnetization reversal. In general, the Nèel DWs are stable configurations in the in-plane ferromagnetic nanostructures. These Nèel DWs are categorized into transverse or vortex depending on the nanowire dimensions. In relatively narrow structures, transverse DW (TDW) is highly stable. The TDWs are characterized as head-to-head or tail-to-tail based on the two domains that it separates [5, 6]. In addition, the TDW has an additional degree of freedom called chirality. The transverse magnetization either pointing "UP" or "DOWN" defines the chirality of the TDW. The DW chirality plays an important role in the DW motion in nanowires [7–13]. Specifically, the DW pinning strongly depends on the chirality [9, 11, 14, 15]. Recently, there has been a lot of interest to explore the DW chirality as a logic bit to execute the binary logic operations for spin-based computation [16]. Goolaup et al. [3] have utilized the DW chirality as a binary bit and demonstrated NOT gate operation by flipping the chirality during the motion in a canted rectangular structure integrated within the nanowire. The field-driven TDW transforms into vortex and back to TDW configurations as per the dimensions. The whole operation flips the chirality of TDW at the output. Omari et al. [12, 16] have shown the

✉ Vijayanandhini Kannan
vkannan@gitam.edu

✉ Chandrasekhar Murapaka
mchandrasekhar@msme.iith.ac.in

✉ Wen Siang Lew
wensiang@ntu.edu.sg

[1] Department of Physics, School of Science, GITAM Deemed to be University, Rudraram, Patancheru Mandal, Hyderabad 502 329, India

[2] Department of Materials Science and Metallurgical Engineering, Indian Institute of Technology Hyderabad, Kandi, Sangareddy 502 284, India

[3] School Physical and Mathematical Sciences, Nanyang Technological University, 21 Nanyang Link, Singapore 637371, Singapore

DW chirality rectification in nanowires designed with constrictions. The chirality-encoded DW-based universal logic operations are realized in the ferromagnetic nanostructures. Current-induced DW motion via spin-transfer torque has attracted significant attention for device applications. The DW speed driven by current reaches a maximum value and drops abruptly due to Walker breakdown [17]. Walker breakdown is a phenomenon, where the DW structure breaks down due to which its speed drops significantly. There are reports in which Walker breakdown has been exploited for DW pinning and depinning at the notches in ferromagnetic nanowires [18]. In addition, J Vandermeulen et al. [19] have exploited the Walker breakdown phenomenon in a nanowire to demonstrate memory and logic operations. The chirality flipping in a nanowire is considered for logic operation. However, identifying the input and output positions is challenging as Walker breakdown largely depends on applied current density. In this work, we explore the Walker breakdown to realize the NOT gate logic operation by flipping the chirality of the TDW driven by the current in a ferromagnetic nanowire with an anti-dot to deterministically position the input and output of the logic functionality. We induce the Walker breakdown at an anti-dot structure that leads to the transformation from TDW to anti-vortex DW and back to TDW. Our design is also capable of bidirectional logic operations. We have systematically investigated the effect of device dimensions and current density for a successful NOT gate logic operation.

1.1 Simulation Method

In this study, we have used a rectangular ferromagnetic nanowire, $Ni_{80}Fe_{20}$ (permalloy) of dimensions with a length of 5 µm, width of 200 nm, and thickness of 10 nm. To study the current-induced NOT gate logic operation, an anti-dot was introduced inside the nanowire. The anti-dot has a rectangular geometry placed at the center of the nanowire with a length of 1 µm with varying anti-dot widths (AD_W) from 20 to 70 nm as shown in schematic Fig. 1a. In addition, we have varied the anti-dot lengths (AD_L) from 0.6 to 1 µm. The presence of anti-dot leads to the nanowire to be seen as two branches above and below, namely the upper and lower branch, respectively. As the anti-dot width is increased, the width of upper and lower branches reduces accordingly. The material parameters are considered for $Ni_{80}Fe_{20}$ (permalloy) where the saturation magnetization, M_s is 860×10^3 A/m, zero magneto-crystalline anisotropy, and exchange constant $A=1.3\times10^{-11}$ J/m [14, 20, 21]. The geometry is divided as a cell size with a unit cell volume of $5\times5\times5$ nm^3 in all our simulations. The cell size of 5 nm is chosen close to the exchange length of permalloy [22]. We used the Object Oriented Micromagnetic Framework (OOMMF) [23] with spin-transfer torque term incorporated to the Landau–Lifshitz–Gilbert (LLG) equation to simulate the current-induced NOT gate operation [6, 24, 25]. The LLG equation including the spin torque can be written as follows:

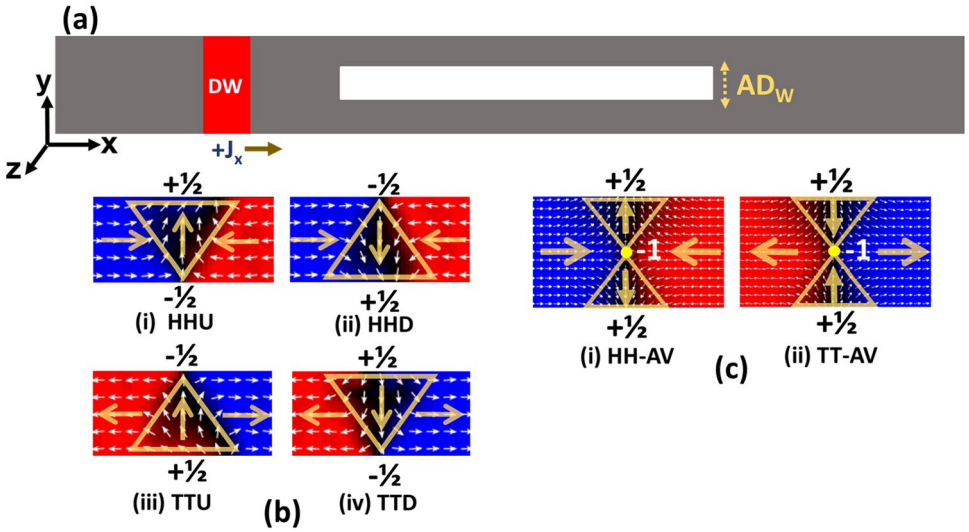

Fig. 1 **a** Schematic representation of the ferromagnetic nanowire with an anti-dot at the center. AD_W stands for anti-dot width. **b** Spin configuration of four possible types of transverse DWs with corresponding winding numbers identified, where (i) HHU is head-to-head spin configuration with "UP" chirality; (ii) HHD is head-to-head spin configuration with "DOWN" chirality; (iii) TTU is tail-to-tail spin configuration with "UP" chirality; and (iv) TTD is tail-to-tail spin configuration with "DOWN" chirality. **c** Spin configuration of two possible types of anti-vortex DWs with corresponding winding numbers identified, where (i) HH-AV is head-to-head anti-vortex DW, and (ii) TT-AV is tail-to-tail anti-vortex DW

$$\frac{\partial \boldsymbol{M}}{\partial t} = -\gamma_0 \boldsymbol{M} \times \boldsymbol{H}_{eff} + \frac{\propto}{\boldsymbol{M}_s} \boldsymbol{M} \times \frac{\partial \boldsymbol{M}}{\partial t} - (\boldsymbol{u} \cdot \boldsymbol{\nabla})\boldsymbol{M} + \frac{\beta}{\boldsymbol{M}_s} \boldsymbol{M} \times [(\boldsymbol{u} \cdot \boldsymbol{\nabla})\boldsymbol{M}] \quad (1)$$

The first term on the right-hand side in the equation relates to the torque exerted on the magnetization vector, M, by the effective magnetic field, H_{eff}. The time lapse (t) for each magnetization configuration snapshot of the DW motion has been recorded. The second term describes the Gilbert damping torque, parametrized by the Gilbert damping constant (α) which is fixed at 0.005 in our simulations. The last two terms are the spin-transfer torque terms which incorporate the two mechanisms, adiabatic and non-adiabatic torques, respectively. The non-adiabatic constant (β) is chosen as 0.04 in our simulations. The effective drift velocity of the conduction electron spins (u) is defined by the following:

$$u = J\frac{g\mu_B p}{2eM_s} \quad (2)$$

where J is the current density, p is the spin polarization which is assumed to be 0.7 in our simulations, M_s is the saturation magnetization, μ_B is the Bohr magneton, e is the electron charge, g is Lande's g factor.

2 Results and Discussion

Figure 1a shows the schematic of the device structure employed for realizing the NOT gate operation. The device structure consists of a rectangular ferromagnetic nanowire with an anti-dot placed at the center. The nanowire dimensions are chosen to stabilize a TDW. We have relaxed a TDW with a specific chirality from the left side of the nanowire, and we have driven the DW using the current-induced spin-transfer torque [6]. The TDW can be either head-to-head (HH) or tail-to-tail (TT) depending on the relative orientation of the two domains it is separating. In addition, TDW can have another degree of freedom which is chirality that depends on the rotation of spins within the DW. If the transverse magnetization of the TDW is aligned towards + Y direction, it is termed as the "UP" chirality, whereas if the transverse magnetization is along − Y direction, it is termed as the "DOWN" chirality. The TDWs are characterized by topological charges (winding numbers) of + ½ and − ½, when all the spins either converge or diverge is represented as + ½ and two spins converge and one diverge or vice-versa is represented as − ½. The spin configuration of all four possible types of TDWs and the two types of anti-vortex DWs with their corresponding winding numbers identified are shown in Fig. 1b and c, respectively. Figure 1b(i–iv) depicts the transverse spin structures of HH DW with UP chirality (HHU), HH DW with DOWN chirality (HHD), TT DW with UP chirality (TTU), and TT DW with DOWN chirality (TTD), respectively. Figure 1c(i) and (ii) shows anti-vortex (AV) spin structures for HH-AV and TT-AV DWs with the corresponding winding numbers, respectively. The anti-vortex core is represented by − 1, whereas the two bases of the triangular spin configuration are represented by + ½ (going with the same definition of topological charges stated above for TDWs) [26].

In this study, the binary bits are assigned to the chirality of the TDW. The UP chirality is defined as "1," and DOWN chirality is defined as "0" to execute the logic functionalities. In order to demonstrate the NOT gate operation, we have relaxed a HHU in the ferromagnetic nanowire and driven along the + X direction by the virtue of the current-induced spin-transfer torque (Fig. 2a). The driving current density (J_x) is fixed at 1.48×10^{12} A/m^2 in all our simulations unless mentioned. The DW reaches the anti-dot and gets pinned at the left edge of the nanowire. The DW initially gets pinned before it gets split into two TDWs of the same type and chirality (in this case, HHU) (Fig. 2b). One of the HHUs stays pinned at the left edge of the anti-dot, while the other HHU progresses through the upper branch due to splitting as shown in Fig. 2c. The DW transverse energy is responsible for this selective depinning mechanism. The DW transverse energy is relatively large at the base of the triangular shape as compared to the vertex [27]. Thus, the DW with base pointing towards the pinning site cannot progress further. However, the DW with vertex pointing towards the pinning site (anti-dot) progresses. Interestingly, the HHU that progresses in the upper branch undergoes a transformation from transverse to anti-vortex state (HH-AV) at the constant current density (Fig. 2d). This phenomenon is famously known as Walker breakdown [28]. The DW once reaches to a maximum speed, the excess energy drives the DW transformation from transverse to anti-vortex state and back to transverse. This transformation occurs periodically leading to an abrupt drop in the DW speed. In this case, the anti-vortex core is nucleated from the vertex of the TDW. The anti-vortex core is associated with − 1 winding number. The nucleation leaves + ½ winding number at the bottom, where it was nucleated. Consequently, there are two + ½ at the bases and one − 1 at the core of the anti-vortex DW. The process follows the conservation of winding number before and after transformation from transverse to anti-vortex state. When an anti-vortex DW (HH-AV) is driven by the current, the core moves transverse to the direction of the DW motion. In this case, the anti-vortex core moves towards + Y direction, leading to the annihilation of the anti-vortex core and leaving behind − ½ vertex at the top edge of the anti-dot. This leads to the transformation of the anti-vortex DW (HH-AV) back to the transverse DW configuration at the other end of the anti-dot. Interestingly, the anti-vortex transforms into HHD flipping the chirality of the initial TDW. This process has flipped the chirality of the HHU into HHD, leading to the transformation of input "1" to output "0" as shown in

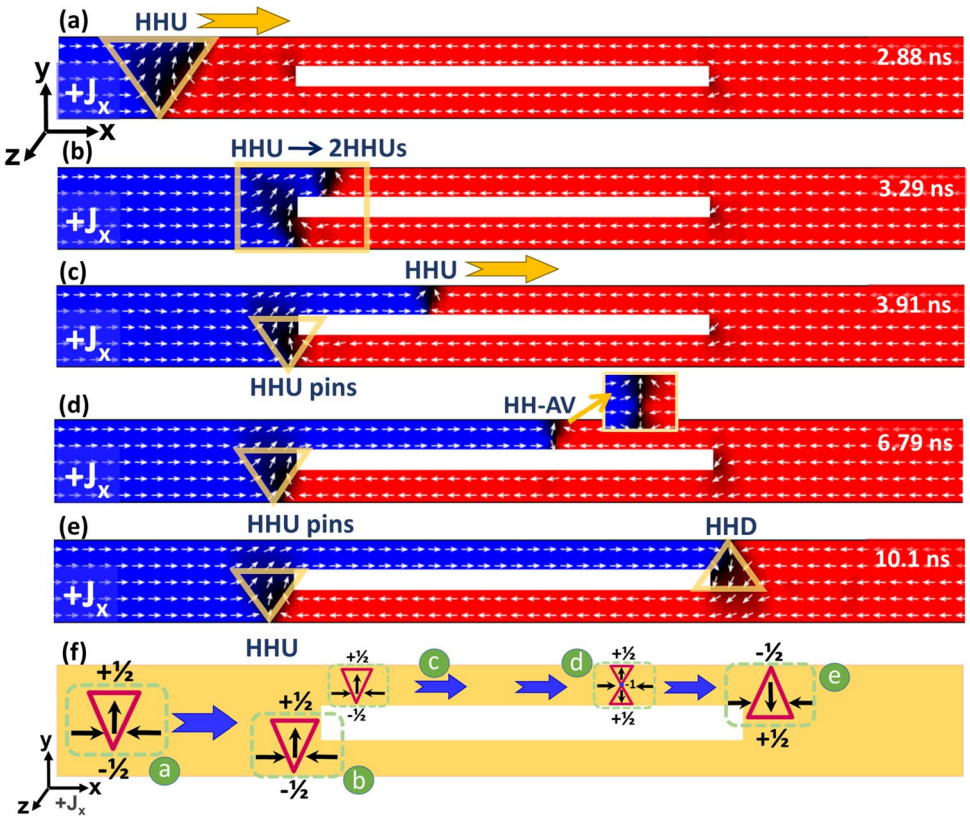

Fig. 2 **a** Snapshot images of the magnetization configuration along with time stamp (as denoted at the right end), when a HHU DW is relaxed and driven by the application of current with current density, J_x, of 1.48×10^{12} A/m^2 along + X direction in the nanowire with AD_W of 50 nm and AD_L of 1 µm; **b** splitting of HHU into two HHUs, wherein one HHU gets pinned at the left side of the lower branch of the AD and the another HHU progresses through the upper branch of the AD; **c** progress of HHU through the upper branch of AD; **d** transformation of HHU transverse DW into HH anti-vortex DW (HH-AV) as shown in zoomed view in the upper branch of the AD; **e** transformation of the HH-AV DW back to the transverse HHD at the other end of the anti-dot showing chirality flipping of HHU to HHD; and **f** schematic representation of the various steps of chirality flipping from HHU to HHD

the schematic with the complete process of various steps (Fig. 2f).

To demonstrate the complete NOT gate logic operation, we have relaxed the DW with opposite chirality as compared to the previous case. As shown in Fig. 3a, we have relaxed a HHD DW in the nanowire and driven towards the anti-dot. Similar to the previous case, the HHD splits into two HHDs at the anti-dot as shown in Fig. 3b. The DW with a vertex pointing towards the anti-dot progresses further owing to the transverse DW energy as discussed above (Fig. 3c). The HHD while progressing in the lower branch transforms into a head-to-head anti-vortex DW (HH-AV) as shown in Fig. 3d. Here, the anti-vortex core is nucleated from the vertex of the TDW similar to the previous case. The anti-vortex core is associated with − 1 winding number. The nucleation leaves + ½ winding number at the top, where it was nucleated. Consequently, there are two + ½ at the bases and one − 1 at the core of the anti-vortex DW. The process follows the conservation of winding number before and after the transformation from transverse to anti-vortex state. The anti-vortex core "− 1" moves transverse with respect to the DW motion along − Y direction. It is to be noticed that the anti-vortex core always moves away from the nucleation point and gets annihilated at the other end of the anti-dot. This leads to the flipping into opposite chirality, HHU (Fig. 3e). This process results in the transformation of input "0" to output "1" as shown in the schematic with the complete process of various steps (Fig. 3f). The whole process results in the successful current-driven DW chirality-based NOT gate logic operation in the proposed device structure.

We have also performed micromagnetic simulations to emulate NOT gate logic operation with TT DW. We have observed TTU flipping into TTD and vice-versa via transformation through the TT anti-vortex DW (TT-AV). The results are shown in Supplementary Information-I and II.

To get an insight on bidirectionality of the device operation, we have relaxed HHU in the right side of the nanowire (Fig. 4). The DW is driven by the current along the − X direction. The DW now gets pinned at the right edge of the anti-dot and gets split as per the transverse DW energy. Similar to the above case, the HHU transforms into an anti-vortex state and back to HHD due to the Walker breakdown (Fig. 4b–e). We have also driven the HHD which turned into HHU via anti-vortex when driven by current in − X direction (Supplementary Information-III). The results highlight the bidirectional functionality of the NOT gate logic operation using this device structure.

To gain insight on the effect of device dimensions on the successful logic operation, we have varied the anti-dot width from 20 to 70 nm and anti-dot length from 0.6 to 1 µm. Figure 5a shows the phase diagram of success and failure cases of the NOT gate operation as a function of anti-dot dimensions. The driving current density, J_x, is fixed

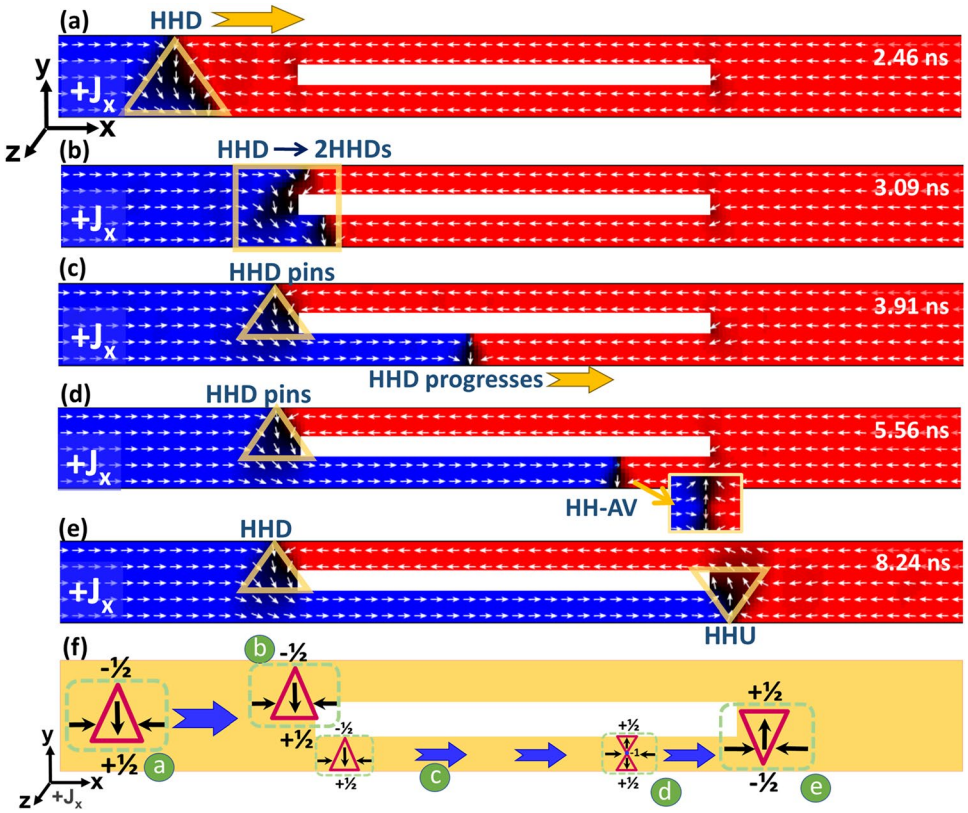

Fig. 3 **a** Snapshot image of the magnetization configuration along with time stamp (as denoted at the right end), when a HHD DW is relaxed and driven by the application of current with current density, J_x, of 1.48×10^{12} A/m^2 along + X direction in the nanowire with AD_W of 50 nm and AD_L of 1 µm; **b** splitting of HHD into two HHDs, wherein one HHD gets pinned at the left side of the upper branch of the AD and the another HHD progresses through the lower branch of the AD; **c** progress of HHD through the lower branch of AD; **d** transformation of HHD transverse DW into HH anti-vortex DW (HH-AV) as shown in zoomed view in the lower branch of the AD; **e** transformation of the HH-AV DW back to the transverse HHU at the other end of the anti-dot showing chirality flipping of HHD to HHU; and **f** schematic representation of the various steps of chirality flipping from HHD to HHU

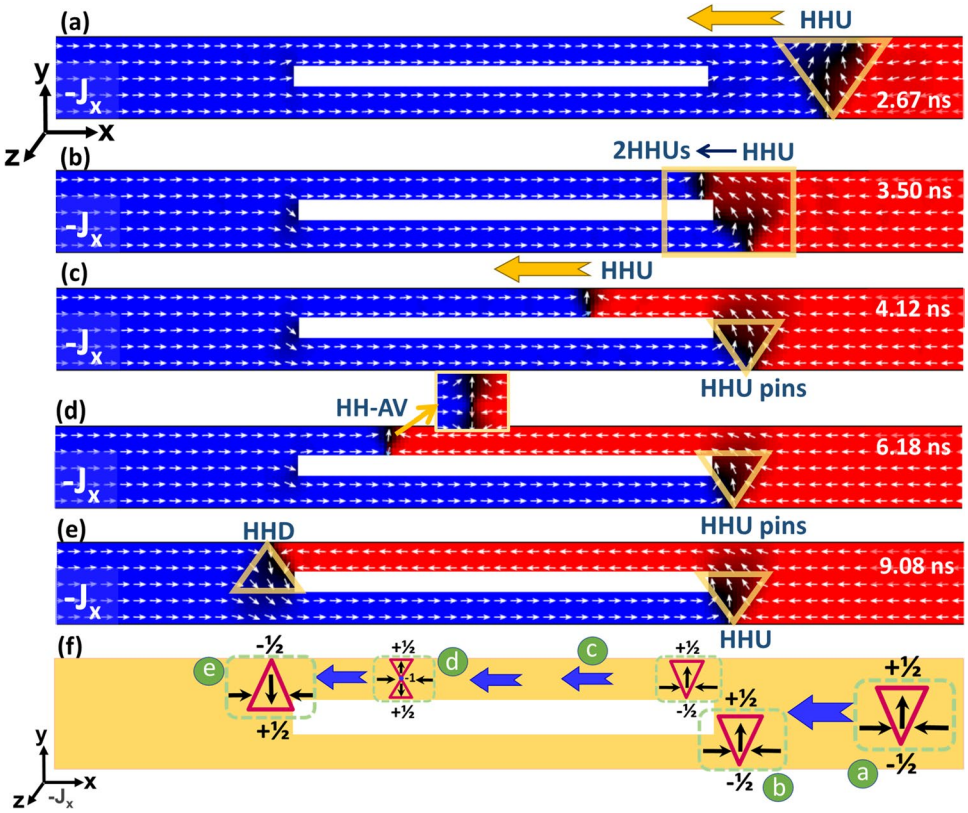

Fig. 4 **a** Snapshot image of magnetization configuration along with time stamp (as denoted at the right end), when a HHU DW is relaxed and driven by the application of current with current density, J_x, of 1.48×10^{12} A/m^2 along − X direction in the nanowire with AD_W of 50 nm and AD_L of 1 µm; **b** splitting of HHU into two HHUs, wherein one HHU gets pinned at the right side of the lower branch of the AD and the another HHU progresses through the upper branch of the AD; **c** progress of HHU through the upper branch of the AD; **d** transformation of HHU transverse DW into HH anti-vortex DW (HH-AV) as shown in zoomed view in the upper branch of the AD; **e** transformation of the HH-AV DW back to the transverse HHD at the other end of the anti-dot showing chirality flipping of HHU to HHD; and **f** schematic representation of the various steps of chirality flipping from HHU to HHD

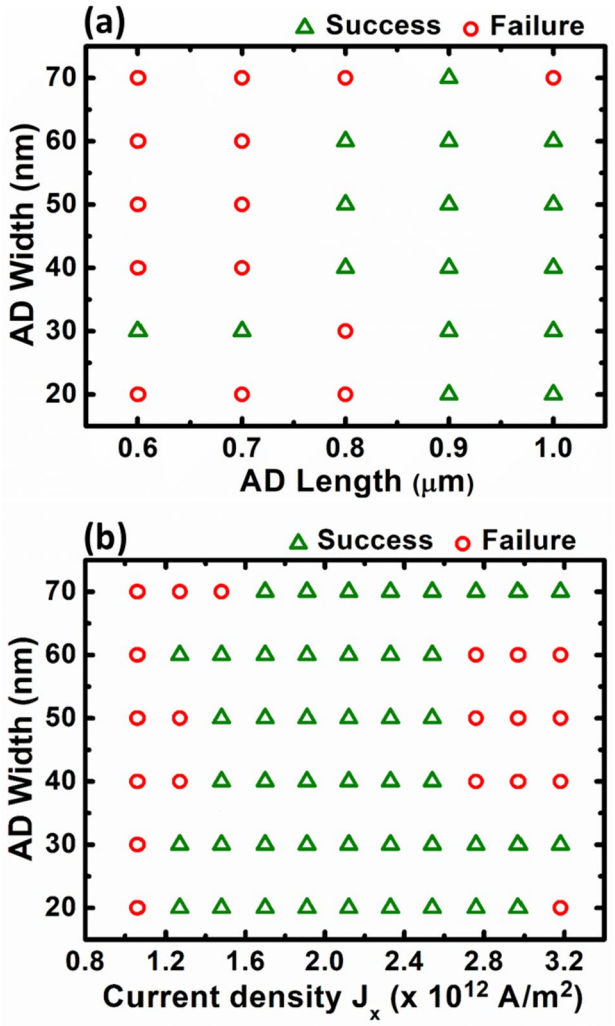

Fig. 5 Working window of NOT logic operation for varying anti-dot (AD) width (nm) as a function of **a** AD length (μm) and **b** current density, J_x, ($\times 10^{12}$ A/m^2) for a fixed AD_L of 1 μm

at 1.48×10^{12} A/m^2 for all cases. The green triangle represents the successful working operation whereas the red circle represents failure. We have observed a successful operation at a relatively larger length of the anti-dot. It is due to the time required for the DW transformation from transverse to anti-vortex and back to transverse during the progression through the branch. For example, at the anti-dot length of 0.6 μm with various anti-dot widths, we observe failure in most cases. This is because the DW splitting takes place at the left edge and one of the DW that progresses reach the right edge even before the transformation from transverse to anti-vortex occurs. In contrast, we have observed a successful operation for AD_L of 0.8 μm and AD_W of 40 nm. This is due to the fact that the DW travels a relatively longer distance before it reaches to the right edge allowing it to transform into the anti-vortex configuration ultimately leading to the chirality flipping. It is interesting to note that the anti-dot width also plays a crucial role for successful operation. When the AD width is relatively low, the probability of success is higher at a particular AD length. However, we have observed failure of logic operation due to the absence of chirality flipping when the AD width is relatively higher. This can be explained from the view of DW speed as a function of AD width. The DW speed at a particular current density largely depends on the branch widths which in turn depends on the AD width. The DW speed reduces as the branch width comes down due to increase in AD width. The DW experiences relatively larger obstruction while progressing through the lower branch widths, causing a drop in their speeds. Thus, the TDW requires to travel longer distances in order to undergo the transformation (or Walker breakdown).

Figure 5b shows the phase diagram corresponding to the successful operation as a function of current density and anti-dot width by keeping the length unchanged at 1 μm. At a relatively lower current density, we have not observed NOT gate operation that is the chirality flipping. The DW chirality stays unchanged while moving through the branch. It means there is an absence of Walker breakdown at relatively lower current densities. For example, at J_x of 1.2×10^{12} A/m^2 and $AD_W = 50$ nm, we observe the absence of Walker breakdown due to lower current densities and low speed of the DW. This can be understood from the DW speed at a particular current density. The DW speed is lower than the threshold speed for the Walker breakdown to take place when the driving current densities are lower. However, when the current density is increased, we have observed successful operation as the DW attains a required speed before it undergoes breakdown. For example, at J_x values of 2.12×10^{12} A/m^2 and $AD_W = 50$ nm, we observe the presence of Walker breakdown and a successful NOT gate logic operation. These observations reveal the importance of Walker breakdown for the DW transformation associated with the chirality flipping to realize NOT gate operation. However, when the current density is higher than 2.8×10^{12} A/m^2, for the same AD width, we have observed failure as the DW speed also scales, and it leads to the multiple transformations between the transverse to anti-vortex, due to Walker breakdown. This makes the logic functionality stochastic that can be either success or failure depending on the dimensions of the nanowire and anti-dot.

3 Conclusions

In summary, we have demonstrated a DW-based NOT gate logic operation enabling the DW chirality as a binary bit. The Walker breakdown caused by the current-driven DW motion is the key in achieving the chirality flipping. Interestingly, the design is suitable for bidirectional operations. The DW transformations from transverse to anti-vortex led to the chirality flipping. The branch width does not support

the stabilization of the anti-vortex due to which it transforms back to transverse, however, with opposite chirality. The dimensions of the anti-dot are found to play a pivotal role via affecting the DW speed and in turn, the chirality flipping. Moreover, the anti-dot length should be chosen suitable for the DW transformation from transverse to anti-vortex back to transverse for successful operation. The relatively low current density does not lead to the Walker breakdown, and the high current density leads to multiple transformations, both resulting to the failure of NOT gate operation.

Supplementary Information The online version contains supplementary material available at https://doi.org/10.1007/s10948-023-06686-2.

Acknowledgements CM would like to acknowledge funding from SERB-Early Career Research Award (ECR/2018/002664). VK would like to acknowledge funding from GITAM—Research seed grants (RSG-2023/0230). RJ would like to acknowledge funding from CSIR-Extra Mural Research (80(0089)/19/EMR-II).

Data Availability Data available on request from the authors.

References

1. Parkin, S.S.P., Hayashi, M., Thomas, L.: Magnetic domain-wall racetrack memory. Science (1979). **320**(5873), 190–194 (2008). https://doi.org/10.1126/SCIENCE.1145799/SUPPL_FILE/PARKIN.SOM.PDF
2. Allwood, D.A., Xiong, G., Faulkner, C.C., Atkinson, D., Petit, D., Cowburn, R.P.: Magnetic domain-wall logic. Science (1979). **309**(5741), 1688–1692 (2005). https://doi.org/10.1126/science.1108813
3. Goolaup, S., Ramu, M., Murapaka, C., Lew, W.S.: Transverse domain wall profile for spin logic applications. Sci. Rep. **5**, 1–8 (2015). https://doi.org/10.1038/srep09603
4. Murapaka, C., Sethi, P., Goolaup, S., Lew, W.S.: Reconfigurable logic via gate controlled domain wall trajectory in magnetic network structure. Sci. Rep. **6**, 1–11 (2016). https://doi.org/10.1038/srep20130
5. Nakatani, Y., Thiaville, A., Miltat, J.: Head-to-head domain walls in soft nano-strips: a refined phase diagram. J. Magn. Magn. Mater. **290–291**, 750–753 (2005). https://doi.org/10.1016/j.jmmm.2004.11.355
6. Thiaville, A., Nakatani, Y., Miltat, J., Suzuki, Y.: Micromagnetic understanding of current-driven domain wall motion in patterned nanowires. Europhys. Lett. **69**(6), 990–996 (2005). https://doi.org/10.1209/epl/i2004-10452-6
7. Jaiswal, R., Haragopal, V., Murapaka, C., Kannan, V.: Chirality-dependent domain wall splitting and recombination in ferromagnetic nanostructure with an anti-dot. J. Supercond. Nov. Magn. **36**(2), 665–673 (2023). https://doi.org/10.1007/s10948-023-06507-6
8. Kondou, K., et al.: Chirality-induced magnetoresistance due to thermally driven spin polarization. J. Am. Chem. Soc. (2022). https://doi.org/10.1021/jacs.2c00496
9. Kim, D.Y., et al.: Chirality-induced antisymmetry in magnetic domain wall speed. NPG Asia Mater **10**(1), e464 (2018). https://doi.org/10.1038/am.2017.216
10. Fillion, C.E.. et al.: Gate-controlled skyrmion and domain wall chirality. Nat. Commun. **13**(1), (2022). https://doi.org/10.1038/s41467-022-32959-w
11. Bisig, A., et al.: Dynamic domain wall chirality rectification by rotating magnetic fields. Appl. Phys. Lett. **106**(12), 1–6 (2015). https://doi.org/10.1063/1.4915256
12. Omari, K., et al.: Ballistic rectification of vortex domain wall chirality at nanowire corners. Appl. Phys. Lett. **107**(22), (2015). https://doi.org/10.1063/1.4936565
13. Dohi, T., Duttagupta, S., Fukami, S., Ohno, H.: Reversal of domain wall chirality with ferromagnet thickness in W/(Co)FeB/MgO systems. Appl. Phys. Lett. **114**(4), (2019). https://doi.org/10.1063/1.5084095
14. Sekhar, M.C., Goolaup, S., Purnama, I., Lew, W. S.: Crossover in domain wall potential polarity as a function of anti-notch geometry. J. Phys. D. Appl. Phys. **44**(23), (2011). https://doi.org/10.1088/0022-3727/44/23/235002
15. Goolaup, S., Low, S.C., Sekhar, M.C., Lew, W.S.: Dependence of pinning on domain wall spin structure and notch geometry. J. Phys. Conf. Ser. **266**, 12079 (2011). https://doi.org/10.1088/1742-6596/266/1/012079
16. Omari, K.A., et al.: Toward chirality-encoded domain wall logic. Adv. Funct. Mater. **29**(10), 1–9 (2019). https://doi.org/10.1002/adfm.201807282
17. Beach, G.S.D., Nistor, C., Knutson, C., Tsoi, M., Erskine, J.L.: Dynamics of field-driven domain-wall propagation in ferromagnetic nanowires. Nat. Mater. **4**(10), 741–744 (2005). https://doi.org/10.1038/nmat1477
18. Huang, S.H., Lai, C.H.: Domain-wall depinning by controlling its configuration at notch. Appl. Phys. Lett. **95**(3), (2009). https://doi.org/10.1063/1.3187530
19. Vandermeulen, J., Van De Wiele, B., Dupré, L., Van Waeyenberge, B.: Logic and memory concepts for all-magnetic computing based on transverse domain walls. J. Phys. D. Appl. Phys. **48**(27), (2015). https://doi.org/10.1088/0022-3727/48/27/275003
20. Purnama, I., Sekhar, M.C., Goolaup, S., Lew, W.S.: Collective motions assisted by magnetostatic interactions in coupled domain wall system. IEEE Trans. Magn. **47**(10), 3081–3084 (2011). https://doi.org/10.1109/TMAG.2011.2158635
21. Purnama, I., Chandra Sekhar, M., Goolaup, S., Lew, W.S.: Current-induced coupled domain wall motions in a two-nanowire system. Appl. Phys. Lett. **99**(15), (2011). https://doi.org/10.1063/1.3650706
22. Purnama, I., Murapaka, C.S., Lew, W.S., Ono, T.: Remote driving of multiple magnetic domain walls due to topological interaction. Appl. Phys. Lett. **104**(9), 1–5 (2014). https://doi.org/10.1063/1.4867468
23. M. J. (Michael J. Donahue 1962-, *OOMMF user's guide [microform] / M.J. Donahue, D.G. Porter*. in NISTIR ; 6376. Gaithersburg, MD: U.S. Dept. of Commerce, Technology Administration, National Institute of Standards and Technology, 1999.
24. Li, Z., Zhang, S.: Domain-wall dynamics and spin-wave excitations with spin-transfer torques. Phys. Rev. Lett. **92**(20), 1–4 (2004). https://doi.org/10.1103/PhysRevLett.92.207203
25. Vanhaverbeke, A., Viret, M.: Simple model of current-induced spin torque in domain walls. Phys. Rev. B. Condens. Matter. Mater. Phys.**75**(2) (2007). https://doi.org/10.1103/PhysRevB.75.024411.
26. Tchernyshyov, O., Chern, G.W.: Fractional vortices and composite domain walls in flat nanomagnets. Phys. Rev. Lett. **95**(19), 1–4 (2005). https://doi.org/10.1103/PhysRevLett.95.197204
27. Zeng, H.T., Petit, D., O'Brien, L., Read, D., Lewis, E.R., Cowburn, R.P.: The influence of wire width on the charge distribution of transverse domain walls and their stray field interactions. J. Magn. Magn. Mater. **322**(14), 2010–2014 (2010). https://doi.org/10.1016/j.jmmm.2010.01.024
28. Lozhkina, O., Reeve, R., Frömter, R., Kläui, M.: Control of the Walker breakdown by periodical magnetic wire-width modulation. J. Appl. Phys. **131**, 233902 (2022). https://doi.org/10.1063/5.0092222